JASA ARTICLE

The performance of time reversal in elastic chaotic cavities as a function of volume and geometric shape of the cavity

Paige E. Simpson and Brian E. Anderson[a)]
Acoustics Research Group, Department of Physics and Astronomy, Brigham Young University, N283 Eyring Science Center, Provo, Utah 84602, USA

ABSTRACT:
Time reversal is used as an energy-focusing technique in nondestructive evaluation applications. Here, it is often of interest to evaluate small samples or samples that do not lend themselves to the bonding of transducers to their surfaces. A reverberant cavity, called a chaotic cavity, attached to the sample of interest provides space for the attachment of transducers as well as an added reverberant environment, which reverberation is critical to the quality of time reversal focusing. The goal of this research is to explore the dependence of the quality of the time reversal focusing on the size and geometric shape of the chaotic cavity used. An optimal chaotic cavity will produce the largest focusing amplitude, best spatial resolution, and linear focusing of the time reversed signal. Ultrasonic elastic-wave experiments are performed on a rectangular, cylindrical, and three-dimensional Sinai billiard prism samples, and experiments are repeated each time these samples are successively cut down to smaller volumes. As the size of the cavity decreases, the peak amplitude may increase or decrease depending on the normalization scheme employed. The higher the degree of ergodicity of the cavity, the higher the amplitude and quality focusing achieved.
 https://doi.org/10.1121/10.0005654
(Received 17 December 2020; revised 1 June 2021; accepted 30 June 2021; published online 21 July 2021)
[Editor: Efren Fernandez-Grande] Pages: 526–539

I. INTRODUCTION

Time reversal (TR) is a signal processing method[1,2] that has three main uses: reconstructing a source event,[3–6] providing an optimal carrier signal for communication,[7–9] and intentionally focusing high energy waves to a point in space.[10–12] TR was originally termed matched signal processing since the waves transit through the system twice, filtering the waves twice.[13,14] TR can be performed in a bounded elastic medium, e.g., a block, using a single source and sensor.[15–17] An impulse response (IR) may be obtained between the source and sensor. If the IR is flipped in time, the broadcast of this reversed impulse response (RIR) creates a time reversed reconstruction of the original impulse at the sensor location. The advantage of using a fixed source and a mobile sensor is that TR focusing can be created wherever the sensor is placed.

There are many different examples of TR being used in elastic media for nondestructive evaluation (NDE).[18–24] In NDE applications, sources are placed at fixed locations and a region of interest on the surface of the sample is selected. A laser may be used as the sensor, aimed sequentially at several points within the region of interest. A full TR experiment is conducted at each sensor location and the nonlinear amplitude dependence of the TR focusing can be used to identify cracks or delaminations. This type of experiment is called the time reversed elastic nonlinearity diagnostic (TREND). TR has also been used in elastic media to locate earthquakes[25,26] and for touchpad technology.[27,28] It is used in fluid media applications, such as room acoustics,[12,29–33] biomedical applications,[34–37] and underwater applications.[8,9,38]

In order to enhance the use of TR for NDE, a chaotic cavity may be used in the setup.[39–41] Chaotic cavities are generally irregular shapes that are used in NDE applications of TR in order to increase peak amplitude (A_p) of TR focusing due to the addition of more reverberation in the IRs. A chaotic cavity is attached (i.e., glued or connected with coupling gel) to the sample under test (a secondary sample or medium). Also attached to the chaotic cavity is the source(s) that broadcasts ultrasound into the cavity. Chaotic cavities are useful when the sample under test is too small to attach transducers to, when it is undesirable to attach transducers to the sample under test, or when the sample under test has a relatively high amount of attenuation (e.g., wood, plastic) and thus not much internal reverberation.

Draeger *et al.*[15,16] theoretically and experimentally explored the idea of using a single source transducer in a chaotic cavity to create a high quality TR focus of elastic wave energy. They showed that they could focus energy to a selected point in space on their chaotic billiard sample with a single channel. Montaldo *et al.*[39] was the first to introduce the idea of using a chaotic cavity to couple energy into another medium. Their chaotic cavity was a duraluminum cube with a partial sphere drilled out of one of the corners, termed a three-dimensional (3D) Sinai billiard. One surface of their cavity was placed in contact with water so that energy focusing could be obtained within the water.

[a)]Electronic mail: bea@byu.edu, ORCID: 0000-0003-0089-1715.

https://doi.org/10.1121/10.0005654

Quieffin *et al.*[40] Also explored using a single source transducer connected to a chaotic cavity to produce spatially localized focusing in water that was comparable to what could be achieved with a beam forming array of source transducers. They explored a contrast parameter that compared A_p to the amplitude of the rest of the focal signal (not including A_p) as a function of whether the signal duration was longer or shorter than the Heisenberg time. Bou Mater *et al.*[41] and Van Damme *et al.*[42] used a chaotic cavity to focus energy into a secondary solid medium with the application to image nonlinear features in the solid medium, i.e., to nondestructively locate cracks within a second sample. They compared the focusing results with traditional TR and deconvolution (inverse filtering) TR, showing the improvement in spatial focusing with deconvolution. They showed that a chaotic cavity transducer could be used to focus energy into a reverberant or a non-reverberant secondary medium. References 10 and 43–46 built upon the idea of chaotic cavities by creating a noncontact acoustic source to excite a solid structure. Their device employed transducers that broadcast airborne ultrasound into an air-filled chaotic cavity that was used with TR to focus energy onto a nearby solid structure. This device was used to focus out-of-plane energy and in-plane energy into a carbon fiber plate to locate a crack and a delamination.[47] None of these studies extensively explored the impact of the size and shape of a chaotic cavity on the quality of the TR focusing of elastic waves.

One study that did explore the impact of sample geometry on elastic wave propagation was that by Lobkis and Weaver[48] who explored the rate of conversion of longitudinal waves to shear waves in various aluminum blocks with the goal to determine how diffuse the sound field was within these blocks as a function of temperature. Their work showed that their cylindrical block had the least diffuse wave field, their rectangular blocks had more diffuse wave fields, and their prism block (a 3D Sinai billiard) had the most diffuse wave field. The more diffuse the wave field is the more chaotic the ray paths are.

There are different types of TR processing methods that have been developed to attain high amplitude focusing, temporally clean TR focusing, and TR focusing with low harmonic distortion. These methods may be used with chaotic cavities. Willardson *et al.*[12] compared five different types of TR processing—traditional, decay compensation, deconvolution, one-bit, and clipping—for room acoustics application. Willardson *et al.* found that clipping TR gave the highest A_p of the TR focus in a reverberation chamber though it did not provide the cleanest focus in terms of temporal quality. Young *et al.*[23] used the same TR processing methods in solid media. They used a fixed size chaotic cavity and compared five different types of TR in order to determine which method gave the highest amplitude of the focus with the least amount of negative side effects. Young *et al.* again found that the clipping TR method yielded the highest A_p. However, they found that decay compensation TR was the best of the five methods for crack detection because it increased A_p compared to traditional TR and introduced the least amount of harmonics (a negative side effect of modifying the IR) compared to other TR methods.

Not much research has been done to determine the impact of the size of the cavity, sample, or room on TR focusing, aside from the work of Ribay *et al.*[29] and Denison and Anderson[31] who studied TR focusing of audible sound in a room. Ribay *et al.* studied TR in a room of fixed size and varied the absorption for different TR measurements. They found that A_p of the TR focus increased proportionally with reverberation time, τ, when the absorption was decreased. Since τ is proportional to room volume, it should follow that A_p will increase proportionally with increasing volume according to their results. They did not study how changing volumes of rooms changes the performance of TR. Denison and Anderson[31] explored two types of changes to rectangular-shaped rooms and the resulting effects on TR performance. They studied the effect on A_p of the TR focus in rooms of different volumes but with the same absorption properties. They also studied identical-sized rooms with different amounts of absorption. Their work confirmed the findings of Ribay *et al.*[29] when the volume of the room was kept constant and the absorption was changed—as they decreased the absorption of the room to increase τ, the A_p increased proportionally. However, when Denison and Anderson[31] changed the volume of the room while keeping the absorption the same, they discovered that A_p was proportional to $e^{-\tau}$ (meaning A_p decreases with increasing volume and with increasing τ) which does not follow a generalized interpretation of Ribay *et al.* for all types of changes to τ. While the work of Denison and Anderson explored the impact of the room size on TR focusing, their experimental evidence of this impact was not extensive, and they did not explore the impact of the shape of the room. Thus further experimental exploration of the impact of the room size (or cavity size) on TR focusing is needed.

The purpose of this paper is to explore the performance of TR, used to focus elastic wave energy to a point in space, as a function of the volume and shape of the cavity (block) under test. Several methods of TR are performed in three aluminum blocks of rectangular, cylindrical, and ergodic (3D Sinai billiard) shapes, and a scan of the spatial dependence of the focusing in each type is measured with a scanning laser Doppler vibrometer (SLDV). This process is repeated for several different volumes of each block as some of the block's volume is removed after each set of scans. This research will help to optimize the size and shape of a chaotic cavity used in TR experiments for NDE applications. The research in this paper essentially combines what Young *et al.*[23] and Denison and Anderson[31] have done by exploring the use of different methods of TR in blocks of different sizes (and shapes). This work can help guide the design of a chaotic cavity in terms of whether the size and shape of the cavity matter.

The peak amplitude, temporal quality, temporal symmetry, spatial quality, spatial clarity, and the spatial full width at half maximum are quantified to explore the quality of the TR focusing as a function of volume. The rectangular

prism represents a convenient shape to manufacture, whereas the cylindrical shape is expected to perform poorly due to it having the least diffuse field, and finally an ergodic shape was chosen to see if its complex geometrical shape is necessary over the use of a more simple rectangular shape. The rectangular and cylindrical cavities may not technically be considered chaotically shaped cavities, but the inclusion of them offers insight into whether the shape matters when designing a chaotic cavity to couple energy into a secondary sample or medium. Additionally, several TR processing methods were explored, including traditional TR, deconvolution TR, clipping TR, and decay compensation TR. The cavities explored in this work were not used to couple reverberant energy into a second sample of interest. Rather it is assumed that higher quality time reversal, i.e., higher A_p and spatial confinement of the focusing, at a location on the cavity surface should translate to better coupling of energy into a secondary sample or medium.

In Sec. II, the following are discussed: the experimental methods used, details of the experimental setup, the difference between the different TR methods employed, sample experiments and results, and the metrics used to quantify and analyze this data. Section III includes results as a function of volume for the different blocks according to the quantification metrics. Section IV provides an analysis of the results in the context of the work of Ribay *et al.* and Denison and Anderson. Section V offers conclusions and suggests further work to be done regarding chaotic cavities in TR studies.

II. EXPERIMENTAL SETUP AND METHODS

A. Experimental setup

A SLDV (Polytec PSV-400) was used to measure the out-of-plane vibrations on the surface of the block under test. This was connected to a Polytec OFV-5000 Controller, which has the velocity output connected to a 14-bit resolution, National Instruments PXI 5122 Digitizer card housed in a National Instruments PXI 1082 chassis. All velocity versus time signals from the SLDV were digitized with a sampling frequency of 500 kHz and were 16 ms in length (8000 samples). Also in the chassis was a National Instruments PXI 7852 R Generator card with four output channels connected to a 50-times gain Tabor Electronics 9400 Power Amplifier. The outputs of the amplifier were connected to APC International piezoelectric transducers of type 851, diameter of 15.70 mm, and thickness of 6.40 mm that were polarized perpendicular to the electrodes (compression mode type). Four transducers were epoxied to each block, which can be seen in Fig. 1. The four source transducers on each block were used in every TR experiment (with their four unique RIRs). The block under test was positioned under the SLDV with the block surface to be scanned located at a height of 26.5 +/− 0.1 cm above the optical table, which is 93.5 +/− 0.1 cm between the top of the block and the front edge of the SLDV head. Each block has a layer of reflective tape on the scanning surface (see Fig. 1). This provides an optimal reflecting surface for the laser light to be reflected back with enough strength into the SLDV to provide a low degree of background noise. Note that the ergodic cavity was positioned on its side for ease of supporting it and the SLDV was shined horizontally from the same distance as with the other samples.

The initial dimensions of the aluminum, rectangular cavity were $24.0 \times 9.4 \times 12.0$ cm (volume of 2707 cm^3). After each set of experiments, the cavity was cut down to reduce the height (initially 24.0 cm) by 2.1 cm with each cut. The smallest cavity measured $5.0 \times 9.4 \times 12.0$ cm (volume of 564 cm^3). The transducers remained fixed at the same locations each time the block was cut, and the focal location was always at the same location (care was taken to ensure this). The area of the surface with reflective tape on it is 112.8 cm^2.

The aluminum, cylindrical cavity initially had dimensions of 12.0 cm diameter and 24.0 cm height (volume of 2714 cm^3). The cylinder was also cut down in height by

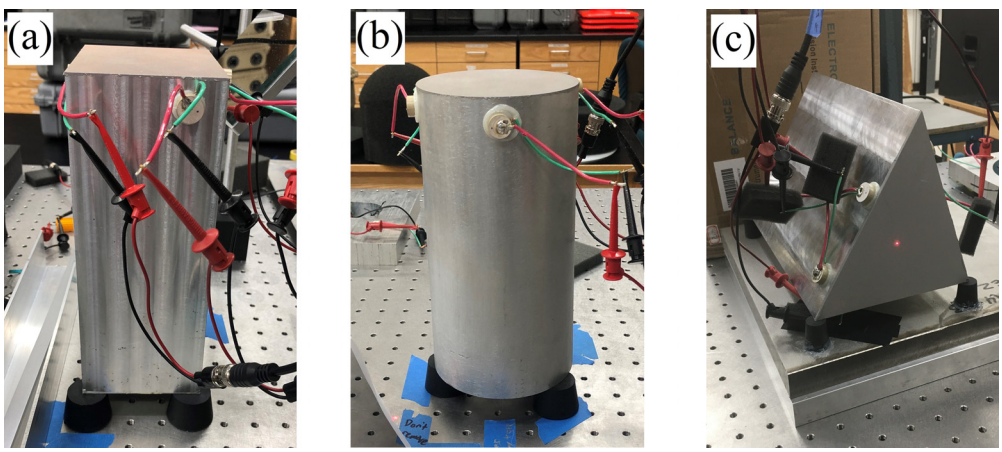

FIG. 1. (Color online) (a) Photograph of the rectangular block positioned under the laser vibrometer (not pictured). On the top surface of the cavity is a layer of reflective tape. Piezoelectric transducers are epoxied to the sides of the cavity. (b) Photograph of the cylindrical block with reflective tape and transducers in the picture. (c) Photograph of the ergodic block with the laser pointing at the location of the focal point.

https://doi.org/10.1121/10.0005654

2.1 cm with each cut. Its transducers and focal location were also fixed at the same locations despite the 24.0 cm height being changed. The smallest cavity measured had the same diameter but with a height of 4.7 cm (volume of 532 cm^3). The area of the surface with reflective tape on it is 113.1 cm^2.

The so-called ergodic cavity (also aluminum), was designed to be similar in shape to the "prism" studied by Lobkis and Weaver.[48] They used ultrasonic waves to find that this type of shape best matched the ray-chaos theory for temperature sensitivity (better than a cylinder or rectangular cavity), which implied the wave propagation was ergodic in nature. An ergodic shape is one that avoids symmetries and parallel walls.[49] Many researchers assert that an ergodic cavity is necessary because the waves are the most randomized when it is used. Ergodicity of a cavity means that every ray of sound will eventually transit every part of the sample, creating a more perfect diffuse field. The ergodic cavity used here is a 3D version of the so-called Sinai billiard (which is often a two-dimensional, 2D, rectangle with a circular perturbation) and is a distorted tetrahedron block with no parallel surfaces and includes two spherical dimples. The block essentially has a triangular cross section (with each leg of the triangle being different) but the two ends are not parallel. The dimples are not quite full hemispheres. Figure 2 displays three photos of the ergodic cavity with its dimensions labeled. The labeled dimensions are $x = 14.6$, $y = 16.2$, $z = 17.9$, $h = 20.35$, $H = 26.25$, $d_1 = 4.7$, $d_2 = 4.85$ cm. Note that the x and y dimensions used here are not the same as those used in the plots of the TR focusing as a function of space. The triangular cross section on the flat end of the block (the end where reflective tape was placed) has an area of 111.7 cm^2. The volume of the block that has this cross section (up to height h) is 2273 cm^3. The volume of the block above height h is a pyramid with a rectangular base (laying on its side) and has a volume of 439 cm^3. The two dimples are spherical caps and were milled out with a 2.54 cm radius ball mill. The volume of the spherical cap near the slanted end with a circular opening of diameter, d_1, has a volume of 16 cm^3. The volume of the spherical cap near the flat end with a circular opening of diameter, d_2, has a volume of 19 cm^3. The volume of the initial ergodic block is therefore the sum of the triangular cross section portion and the pyramid portion minus the two spherical cap volumes and is calculated to be 2678 cm^3. After each set of TR measurements, each cut preserved the angle of the slanted end but removed 2.1 cm off the heights h and H of the block such that the angle of the slanted end is preserved. The h and H dimensions were measured after each cut and the volume was recalculated using the method just mentioned (except that one dimple was removed after a few cuts). The mass of the initial block was measured to be 7568 g and then 7620 g after the piezoelectric sources and reflective tape were added. The density of the aluminum blocks was calculated to be 2824 kg/m^3. After each cut, the mass of the block was measured again and, using the calculated density, the volume of the block was determined. The volumes determined from the geometry calculations and from the mass measurements agreed to within an average of 0.3%. The final volume of the ergodic cavity was 589 cm^3.

The precise type(s) of waves used in these experiments was not determined. It is assumed that the spatial extent of the surficial focusing is dominated by Rayleigh waves and the depth of the focusing would be dominated by shear waves. This is because the frequencies employed, cavity dimensions, and cavity material are very similar to those used by Remillieux *et al.*[50] The dominant Rayleigh wave speed is approximately 2910 m/s and the central frequency wavelength is approximately 29.1 mm for 100 kHz.

After each set of TR measurements was completed, the block was cut down and the block was replaced such that the standoff distance between the SLDV and the block surface was the same to try to maintain the same number of scan points. The scan grid was intentionally made larger than the block surface such that one or two rows or columns of scan points were off of the block. A rectangular grid of scan points was always used. The grid spacing was identical in both dimensions. For the rectangular block, the grid measured 13.0 by 10.4 cm^2 with 65 by 52 points. Thus, the average grid spacing was 2.0 mm (or 14.6 points per

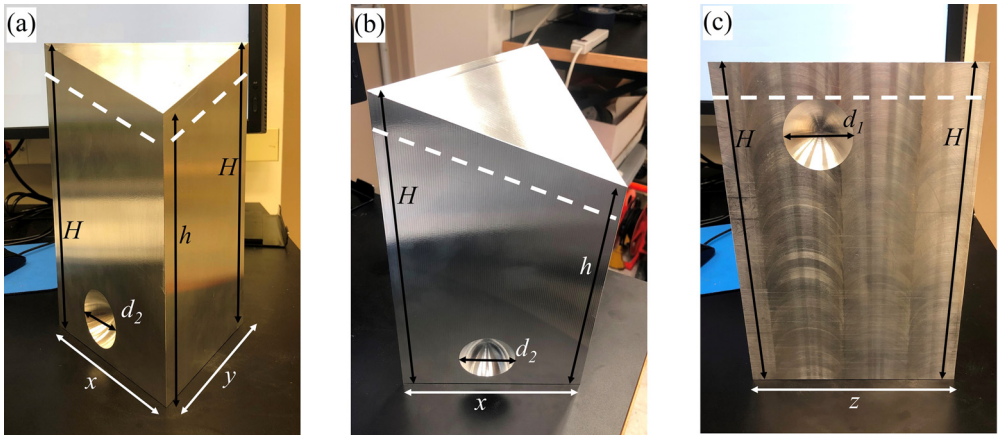

FIG. 2. (Color online) Photographs of the ergodic block from different angles with the dimensions identified. The surface on which the reflective tape was applied, and on which the scans were done, is the bottom of the block as pictured.

wavelength). The focal position was (78, 42 mm) and the focal time was 14.0 ms. For the cylindrical block, the grid measured 13.5 by 13.4 cm^2 with 70 by 70 points. The average grid spacing was 1.9 mm (or 15.1 points per wavelength). The focal position was (55.7, 50.0 mm) and the focal time was 14.0 ms. For the ergodic block, the grid measured 15.4 by 16.0 cm^2 with 80 by 84 points. The average grid spacing was 1.9 mm (or 15.2 points per wavelength). The focal position was (76.6, 57.4 mm) and the focal time was 14.0 ms. These focal locations were chosen in order to not be directly in line with the axis of any of the transducers and avoid the geometric center of the surface of the block to avoid any glaring symmetries in the TR focusing.

B. Time reversal methods

Four different types of TR methods are explored here: traditional, deconvolution, clipping, and decay compensation. Traditional TR is just the IR flipped in time; there are no other modifications made to the signal response other than normalizing the RIR before amplifying it. The other three types of TR utilize modified versions of the IR. Deconvolution TR, or inverse filtering TR, is a method that results in a spatially clean TR focal map that also has hardly any temporal side lobes in the focal signal.[51–53] However, A_p is greatly reduced in amplitude to achieve that clean TR focus. The purpose of deconvolution TR is to minimize of the effects of system resonances in the traditional, "matched signal," TR process. One-bit TR[54] (not explored in this paper) is a process in which the data samples in the RIR are set to be either 1 or −1. One-bit TR preserves the phase information in the RIR (the timing of the reflections) but provides a TR focusing signal with a high A_p and large temporal side lobes. Clipping TR is a slight variant of one-bit TR, in which a threshold is defined such that all values below the chosen threshold maintain their original amplitudes, and all values above the threshold are set equal to the threshold.[55] Thus, the low-amplitude portion of the RIR, which has a lower signal-to-noise ratio, is not amplified by as much as the higher amplitude portion of the RIR that has a larger signal-to-noise ratio. Clipping TR produces a focal signal that is similar to one-bit TR but with a slightly higher A_p. Clipping TR used here employed a threshold of 0.02 as suggested by Young *et al.*[23] Decay compensation TR compensates for the exponential decay of the impulse response by using the envelope of the RIR to adjust the modified IR's amplitude.[12,23,56] In order to achieve this goal, the envelope is inverted, can be smoothed, and then multiplied by the RIR point by point. Thus, the modified RIR is amplified in a similar manner to one-bit or clipping but the tops of the signal have not been clipped as dramatically, hence why less harmonic distortion is introduced in decay compensation TR than with one-bit TR or clipping TR.[23]

C. Sample experiment and result

A linear chirp signal spanning from 75 to 125 kHz is used in the forward step with an input voltage of 750 mV in order to extract the IR (through a cross correlation operation)[32,42] between each transducer and the selected focus location. The chirp signal, an example recording of the chirp signal by a transducer, and the extracted impulse response are displayed in Figs. 3(a) and 3(b). Those IR signals were reversed in time and sent through the respective transducers with an input voltage of 250 mV for traditional TR, 100 mV for clipping TR and decay compensation TR, and 1 V for deconvolution TR to create the TR focus at the selected focus location on a given block. The various input voltages were selected to maintain the same dynamic range on the analog to digital conversion with similar TR focal amplitudes. The TR focusing was assumed to be done at sufficiently low amplitudes that linear scaling would be expected. Thus, the differences in input voltages for the broadcast of the reversed IRs were removed through linear scaling when computing the TR focusing metrics. It is important to note that the RIR signals are normalized with respect to their peak values, irrespective of the TR method employed, before amplifying them to maximize the gain from the amplifier. These RIR signals were sent through the amplifier to the transducers multiple times for averaging purposes (50 averages were used) at each scan location. The SLDV measured the velocity response at various scan points on the block's surface to measure the spatial dependence of a single TR focus. Traditional TR and deconvolution TR were conducted on all three blocks for each of the volumes studied. Clipping TR and decay compensation TR were only conducted on the rectangular block for all of the volumes studied.

After data were collected from a given scan, it was processed using MATLAB to calculate the TR quality quantification metrics described below. Results from a sample experiment conducted on the rectangular block with a cut down volume of $9.2 \times 9.4 \times 12.0$ cm can be seen in Fig. 3. The results shown in Fig. 3 are plots of the amplitude vs time at the focal location for the four different methods of TR. Deconvolution TR gives the cleanest signal but has the lowest amplitude. Clipping TR gives the highest A_p but has high amplitude side lobes. A comparison of these TR methods is given in Sec. III. A similar in-depth comparison of these TR methods for a flat cylindrical sample was conducted by Young *et al.*[23]

Figure 4 shows sample maps of the velocity amplitude as a function of spatial position at the time of peak TR focusing for each of the three blocks at their respective initial volumes. Since the scan area included several points that were not on the block, the SLDV registered very noisy signals at those locations (because the laser light is not reflected back to the detector), as can easily be seen in the corners of the image in Fig. 4(b). Since some of the TR quality metrics studied here involve spatial comparisons of the focal amplitude to the amplitudes elsewhere on the block, a procedure was developed to quantify the amplitude of the focal signals at the beginning of the time window where the points off of the block would have very large noise but the points on the block would have very little noise or signal. A selected threshold allowed identification of the

https://doi.org/10.1121/10.0005654

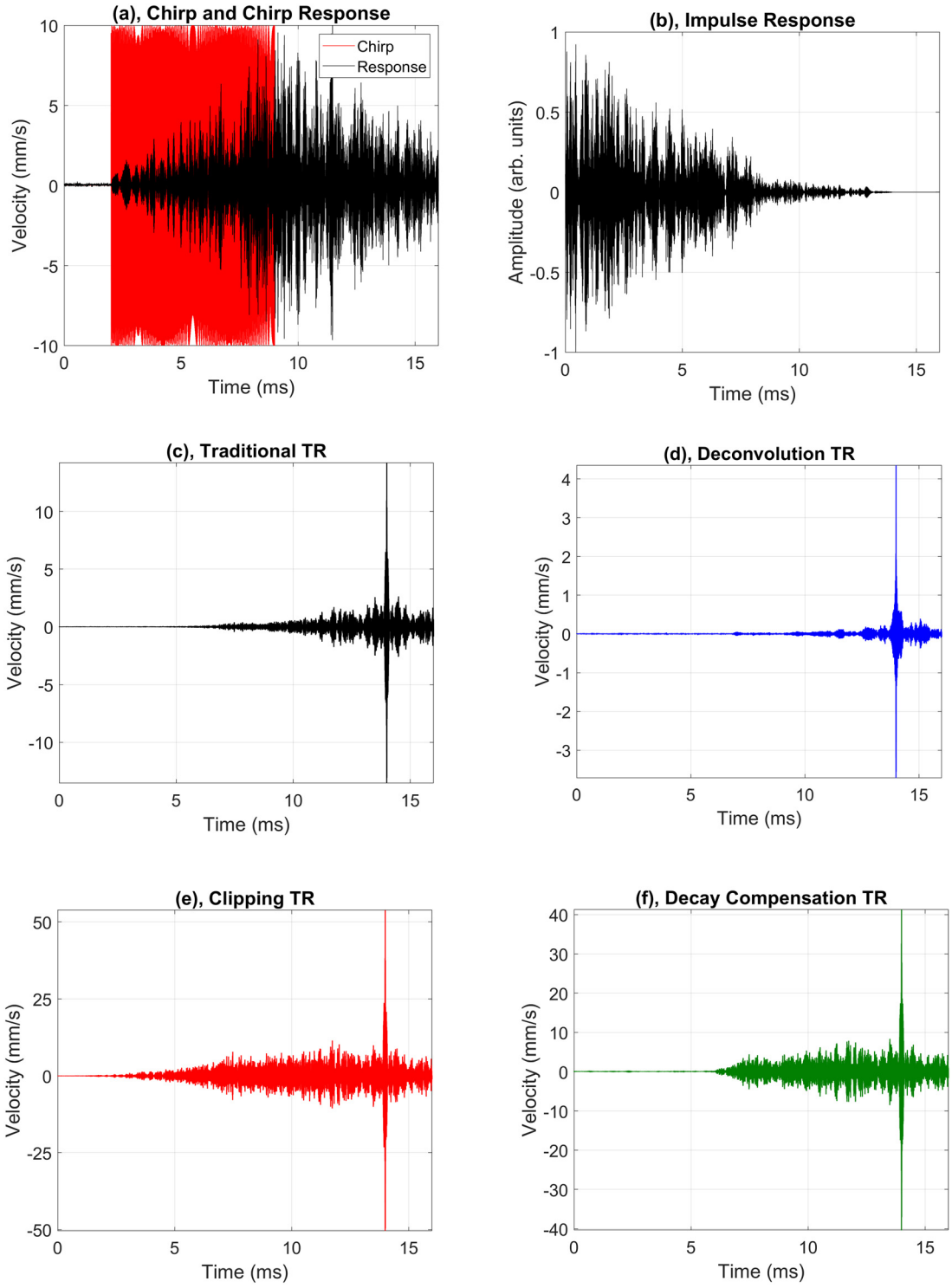

FIG. 3. (Color online) Representative signals of the time reversal process conducted on the rectangular block. (a) The chirp signal and the response to the chirp signal are displayed. (b) The normalized impulse response obtained from a cross correlation of the chirp signal and the response to the chirp signal. (c) A typical traditional TR focus signal. (d) A typical deconvolution TR focal signal. (e) A typical clipping TR focal signal. (f) A typical decay compensation TR focal signal.

points off the block and then those time signals for the scan positions identified as being off the block were set to zero for all time samples. Figure 4(c) shows a scan result where the upper corners of the image are smooth in contrast to Fig. 4(b). The shape of the flat surface on the end of the ergodic cavity (the triangular cross section) is clearly identifiable in Fig. 4(c). Occasionally a few scan points off of the block were not properly identified, perhaps because the laser light reflected off of something that provided enough light back into the detector.

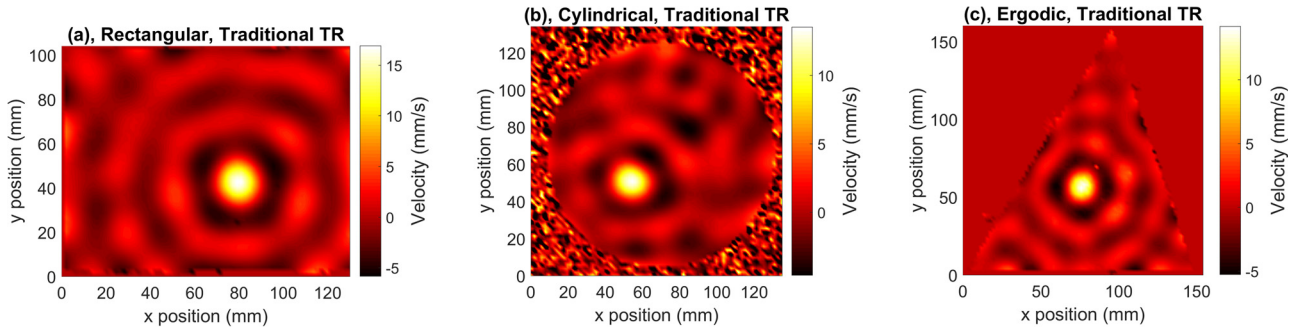

FIG. 4. (Color online) Representative maps of the velocity amplitude as a function of position at the time of peak focusing on the (a) rectangular block, (b) cylindrical block, and (c) ergodic block when traditional time reversal is used. The location of the focus is at (78.0, 42.0 mm), (55.7, 50 mm), and (76.6, 57.4 mm) for the three blocks, respectively. When the laser is not shining on the block the recorded signal is very noisy and this noise is included for the image in (b) (for visualization purposes but it was eliminated in the analysis), but in (a) and (c) the noisy data points have been zeroed out.

D. Analysis quantification metrics

The main metric of interest in the use of a chaotic cavity for nonlinear NDE techniques is the A_p of the TR focus. By changing the size and shape of the blocks and repeating the experiments, the hope is to determine the relationship between A_p and cavity volume and shape. Additional metrics such as temporal quality,[31,55] temporal symmetry,[57] spatial quality,[55] spatial clarity,[31] spatial full width at half maximum (FWHM), and Heisenberg time[31,49,58] all help to characterize the TR focusing.

Temporal quality, ξ_T, is a metric that compares ${A_p}^2$ to the sum of the squared amplitudes throughout the focal signal $f(m)$,

$$\xi_T(x_0,y_0)=\sqrt{\frac{[A_p]^2}{\sum_{m=1}^{M}[f(m)]^2}}, \tag{1}$$

where m is an individual time sample. Here, we remove the $1/M$ factor [compare to Eq. (4) in Ref. 27] so that the ξ_T does not depend on the number of samples in the focal signal, M, and is instead bound between values of 0 and 1. The perfect TR focal signal would be a delta function, which would have $\xi_T=1$. The higher the ξ_T, the cleaner the temporal focal signal is because the side lobes are relatively small in amplitude compared to A_p. ξ_T is similar in nature to the contrast parameter used by Quieffin *et al.*,[40] except ξ_T includes A_p in the denominator, whereas the contrast parameter does not.

Temporal symmetry, Σ_T, is a measure of the similarity of a portion of the focal signal before the time of A_p to an equal-duration portion of the focal signal after the time of A_p.[57] TR is a temporally symmetric process, so the higher the degree of symmetry, the higher the quality of TR focusing. A perfectly symmetric signal would have a $\Sigma_T=1$.

Spatial quality, ξ_S, compares ${A_p}^2$ to the sum of the squared amplitudes elsewhere in space. ξ_S operates on the spatial dependence at the focal time on amplitude maps, $A(x,y)$, such as those shown in Fig. 4,

$$\xi_S=\sqrt{\frac{[A_p]^2}{\sum_{n_x=1}^{N_x}\sum_{n_y=1}^{N_y}[A(x,y)]^2}}. \tag{2}$$

Here again, we remove the factor $1/(N_xN_y)$ [compare Eq. (7) in Ref. 43] such that ξ_S does not depend on the number of scan points used and is bound between 0 and 1. The scans on the different blocks have different numbers of scan points, hence why removing the $1/(N_xN_y)$ factor is useful.

Spatial clarity, Λ_S, compares the $\xi_T(x_0,y_0)$ at the focal location (x_0,y_0) to the $\xi_T(x,y)$ of the rest of the scan points to show how significant the impulsive focusing is at the focus location

$$\Lambda_S=\sqrt{\frac{[\xi_T(x_0,y_0)]^2}{\sum_{n_x=1}^{N_x}\sum_{n_y=1}^{N_y}[\xi_T(x,y)]^2}}. \tag{3}$$

Again, we remove the $1/(N_xN_y)$ factor [compare with Eq. (5) of Ref. 27] here so that Λ_S does not depend on the exact number of scan points used (N_x and N_y are the number of scan points in the x and y directions). Removing this factor also ensures that Λ_S is bound between 0 and 1. ξ_S is similar in purpose to Λ_S except that the spatial evaluation for ξ_S is only considered at one instant in time.

The spatial dependence of the focusing at the focal time of A_p was determined for a horizontal slice and a vertical slice through the spatial map of the amplitude at the focal time $[A(x,y)]$. The full width at half maximum (FWHM) of the squared amplitudes in each slice was then averaged. This metric gives insight into the spatial resolution of the focusing. In diffraction theory, the FWHM cannot be smaller than a half wavelength.

Heisenberg time is calculated for each volume of the block and is proportional to modal density and thus related to the spacing between modal frequencies. A more detailed description is given in Sec. III. Essentially, the calculated

https://doi.org/10.1121/10.0005654

Heisenberg time is longer than τ and the acquisition time (16 ms) for recording the IRs and the focal signals, meaning that the wave fields used in these experiments can be considered diffuse.

III. RESULTS

The A_p is extracted from the focal signal after applying a custom interpolation technique that employs zero padding. This obtains a better estimate of A_p by avoiding issues related to sampling frequency and discrete quantization of samples. To do this, a Fourier transform of the focal signal is computed. In MATLAB, this spectrum contains content from zero frequency up to the Nyquist frequency, and then this content is mirrored between the Nyquist frequency and the sampling frequency. Zeros are then artificially added between the portion of the spectrum from zero frequency up the Nyquist frequency and the portion from the Nyquist frequency up to the sampling frequency. In this case, the modified spectrum is made to have 16 times the number of discrete values as it originally had, with the middle of the modified spectrum having values of zero. An inverse Fourier transform is calculated; the real part of this result is multiplied by 16. The result is an interpolated focal signal with 16 times the number of time samples as the original focal signal and it allows for an estimation of the peak amplitude.

The A_p as a function of volume is plotted in Fig. 5 for each of the three samples when using traditional TR and deconvolution TR (the "Peak Norm." data). Note that the "No Norm." data in Fig. 5 will not be discussed until midway through Sec. IV. A linear fit was applied for each of the plots of A_p versus volume. There is a positive correlation coefficient (with a linear fit) of $R = 0.73$ for the traditional TR method between the volume of the rectangular block and A_p. This implies that as volume increases, A_p increases also. However, for the cylindrical and ergodic blocks, A_p does not increase with increasing volume and instead may slightly decrease with increasing volume (linear fit correlation coefficients of $R = -0.29$ and $R = -0.32$, respectively). There are fluctuations in the data of A_p as a function of volume. These fluctuations likely stem from the peak normalization procedure employed. The RIRs were normalized with respect to their peak amplitudes, and the peak amplitudes of these RIRs generally do not correspond to the direct sound, which should remain the same for each volume. For deconvolution TR, the rectangular, cylindrical, and ergodic blocks had correlation coefficients of only $R = 0.34$, $R = -0.01$, and $R = -0.01$, respectively. Thus, whether A_p may increase or decrease with increasing volume is not easy to determine from these data since the correlation coefficients are not very large or are essentially zero, suggesting that, in general, the dependence of A_p on volume is either not strong or non-existent. In Sec. IV, we discuss an alternative analysis that simulates removing the peak normalization and a very different conclusion is drawn. As expected, clipping TR and decay compensation TR methods yield consistently higher values of A_p than achieved with traditional TR and deconvolution TR methods in the rectangular block. Also, traditional TR yields a higher A_p than does deconvolution TR by about a factor of 3.1 as reported previously by Anderson *et al.*[53] and as shown more clearly in Fig. 6(a).

The temporal and spatial metrics—FWHM, symmetry, temporal quality, spatial clarity, and spatial quality—for traditional TR and deconvolution TR for all three blocks are plotted in Fig. 6. The average values of the metrics (averaged over volume) are given in Table I. The spatial width of the focus, as quantified by FWHM, is 6% wider when using deconvolution TR techniques than traditional TR techniques. There is generally not a correlation between the volume of the block and FWHM over the range of volumes tested. The symmetry of the traditional TR focal signals is 14% higher than when using deconvolution TR. Symmetry also does not have a strong correlation with volume of the block. Temporal quality is 69% higher when using deconvolution TR techniques but also has very low correlation to changes in volume. The symmetry and temporal quality improvements are expected with the cleaner TR focal signals that result from deconvolution TR. Spatial quality is 6% higher using deconvolution TR techniques. Spatial quality has little correlation with volume for traditional TR, but for deconvolution, TR has correlation coefficients of 0.85, 0.60, and 0.66 for the rectangular, cylindrical, and ergodic blocks, respectively. This suggests that as the block volume increases, the spatial quality of deconvolution TR increases. Finally, with spatial clarity, the deconvolution TR technique yields 41% higher values than with traditional TR. The correlation coefficients are not very large but there is some correlation of an increasing spatial clarity with increasing volume. This analysis suggests that the quality of the TR spatial focusing improves somewhat with increasing volume of the block but the A_p and temporal metrics do not seem to be correlated with the block volume for the volumes studied.

The ergodic block consistently yields the largest A_p, with the rectangular and cylindrical blocks yielding similar values for A_p. Interestingly, the FWHM results from the cylindrical block yield the narrowest spatial width, followed by the ergodic block, with the rectangular block yielding the largest FWHM. These results may depend on the selected location for focusing due to the geometry of the sample. The symmetry and temporal quality results for the ergodic cavity are ever so slightly larger than those for the rectangular and cylindrical blocks on average. The spatial quality and spatial clarity results for the ergodic block are 17% and 13% larger on average than for the corresponding results on the other two blocks. Thus, the ergodic geometry of the block generally leads to a higher A_p and a higher quality of spatial focusing compared to the cylindrical and rectangular geometry blocks.

The Heisenberg time, t_H, is proportional to the modal density.[40,41,48,49] Thus, the longer t_H is the more diffuse the wave field because the modal density is higher. Weaver indicates that if the duration of the experimental acquisition time is longer than t_H, then it is as if the acoustic system has resolved each of the discrete modes.[59] In other words, after t_H waves have already traveled through every portion of the

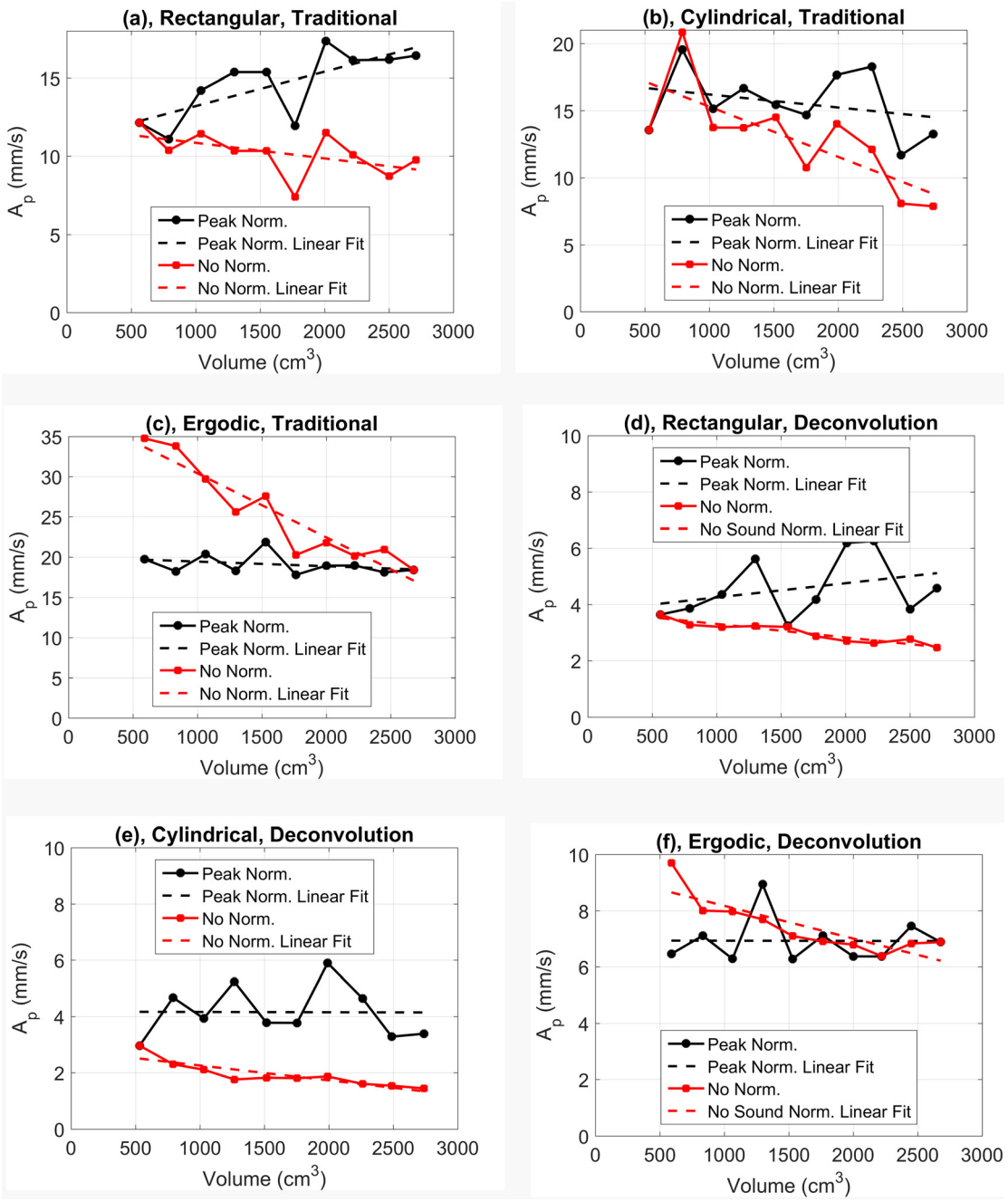

FIG. 5. (Color online) Peak amplitude vs volume of the TR focusing on the three different blocks with traditional TR and deconvolution TR focusing techniques. Shown are the results when normalizing the impulse response using the peak amplitude in the signal (labeled "Peak Norm." with black colored circles) and the results when not using normalization (labeled "No Norm." with red colored squares). Finally, linear fits to the results are also included (dashed lines). (a) Traditional TR on the rectangular block. (b) Traditional TR on the cylindrical block. (c) Traditional TR on the ergodic block. (d) Deconvolution TR on the rectangular block. (e) Deconvolution TR on the cylindrical block. (f) Deconvolution TR on the ergodic block.

sample, the waves can only then retrace paths they have already traveled. It is thus not useful to record an impulse response longer in duration than t_H. For an elastic medium, t_H varies with volume, surface area, and frequency. The shortest t_H we calculated, based on a derivative with respect to frequency of an equation for the number of modes in a rectangular elastic cavity given by Weaver,[60] was 25.5 ms for 75 kHz. This was for the smallest volume tested. This time of 25.5 ms is longer than the acquisition time and is longer than τ. For the largest volume, $t_H = 106$ ms, and again the acquisition time and τ were smaller than this value. Thus, it is reasonable to assume that wave field in each of our rectangular cavity volumes is diffuse and the modes are not yet resolved.

It is assumed that the blocks of different geometrical shapes should still have approximately the same reverberation times, τ. Using the impulse responses extracted from each of the transducers on each of the blocks, average τ

https://doi.org/10.1121/10.0005654

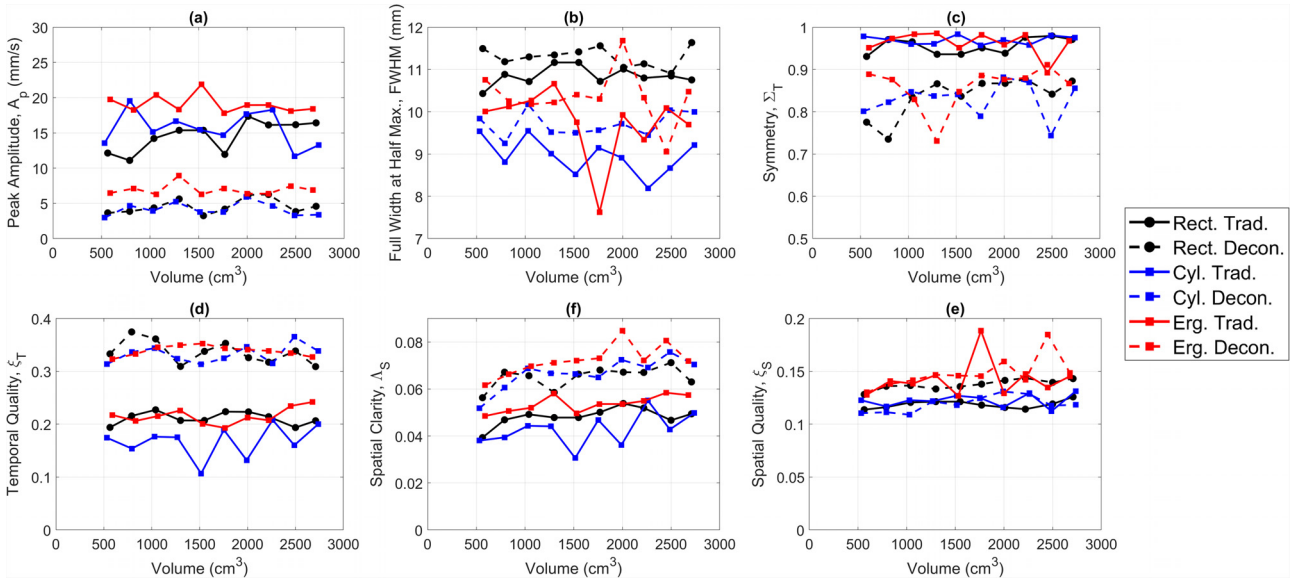

FIG. 6. (Color online) Various metrics to quantify the quality of the TR focusing compared to volume on each of the three blocks when using traditional TR and deconvolution TR. (a) Peak amplitude of the TR focusing, A_p. (b) Full width at half maximum of the spatial extent of the TR focusing. (c) Symmetry of the TR focus signal, Σ_T. (d) Temporal quality of the TR focus signal, ξ_T. (e) Spatial clarity of the spatial dependence of the TR focusing, Λ_S. (f) Spatial quality of the spatial dependence of the TR focusing, ξ_S.

were extracted. τ was measured using reverse Schroeder integration. The τ was averaged across the 4 transducer channels. τ as a function of volume for each of the three geometrical shapes is plotted in Fig. 7(a). It is clear that τ generally increases with increasing volume for each of the blocks with correlation coefficients of 0.89 for the rectangular block, 0.78 for the cylindrical block, and 0.93 for the ergodic block. It is also apparent that the τ are similar across the three block shapes at each volume. The ergodic and cylindrical block τ are on average only different by 2%. The rectangular block τ are 9% and 11% less than those for the cylindrical and ergodic blocks, respectively. Thus, the results for the TR metrics are not likely due to differences in τ.

The piezoelectric transducers used on each of the blocks were the same type and same dimensions and were placed approximately the same distances from the focal location. Using the impulse responses discussed in the previous paragraph, an attempt was made to quantify the amplitude of the direct sound from each of the impulse responses. The transducers were approximately 9 cm on average away from the focal location. Thus, the average amplitude of each impulse response over the first 31 μs, or 15 samples (9 cm/2910 m/s $= 31\mu$s, where 2910 m/s is the Rayleigh wave speed), was determined (averaged over the first 15 samples). This average amplitude for each impulse response was then averaged over the four transducers and a plot of the average direct sound amplitude as a function of volume for the three different blocks is plotted in Fig. 7(b). Arbitrary units for the amplitude are used since the impulse responses extracted from the cross correlation operations were not adjusted to be in absolute units. The direct sound amplitude does not appear to depend on volume as expected. The average peak direct sound amplitudes are 2680, 3100, and 2810 for the rectangular, cylindrical, and ergodic blocks, respectively, meaning they are within 15% of each

TABLE I. Average values of the various metrics quantified in this study (averaged over volume) for the three different blocks studied and for both traditional TR and deconvolution TR. Since the metrics did not change much with volume, a comparison by shape seemed more appropriate. The rectangular values are given in absolute numbers, while the values for cylindrical and ergodic are given as ratios with respect to the rectangular values (for each given TR method). For example, the cylindrical block yielded a peak amplitude 1.07 times higher than the rectangular block for traditional TR and the cylindrical block yielded a peak amplitude 0.91 times lower than the rectangular block for deconvolution TR.

	Traditional TR			Deconvolution TR		
	Rectangular	Cylindrical	Ergodic	Rectangular	Cylindrical	Ergodic
Peak Amplitude, A_p (mm/s)	14.6	1.07	1.31	4.58	0.91	1.51
Full Width at Half Maximum, *FWHM* (mm)	10.8	0.83	0.90	11.3	0.86	0.92
Temporal Symmetry, $\sum_T$	0.96	1.01	1.01	0.84	0.99	1.03
Temporal Quality, ξ_T	0.2113	0.79	1.02	0.3361	0.99	1.01
Spatial Quality, ξ_S	0.1186	1.03	1.20	0.1376	0.87	1.08
Spatial Clarity, Λ_S	0.0483	0.88	1.11	0.065	1.03	1.11

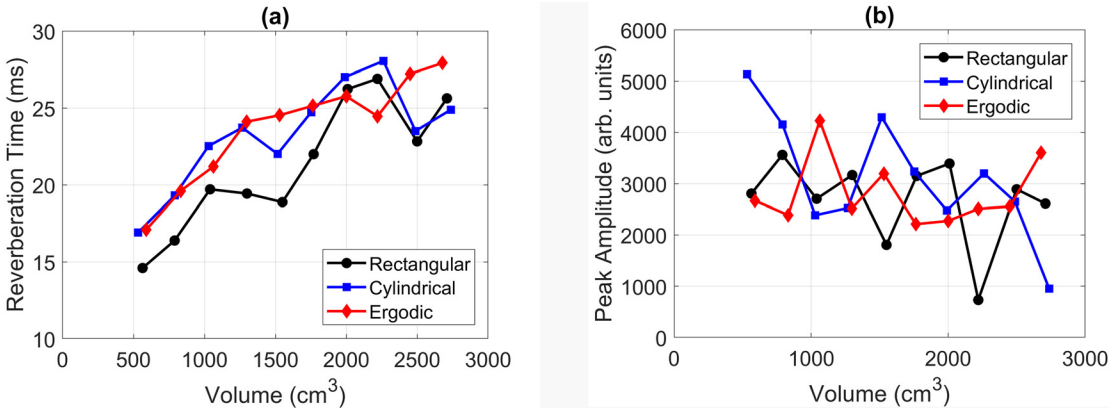

FIG. 7. (Color online) (a) Average reverberation time as a function of volume and block geometry extracted from impulse responses. (b) Average direct sound amplitude as a function of volume and block geometry extracted from impulse responses.

other. Again, the TR metrics reported here likely do not greatly depend on the use of more efficient transducers on one block over another.

IV. DISCUSSION

The finding of an increase in A_p with increasing volume, and increasing τ, in the traditional TR experiments conducted on the different volumes of the rectangular aluminum block seems to agree with the assertion of Ribay *et al.*[29] and disagree with the findings of Denison and Anderson.[31] Each of these two former studies employed traditional TR and rectangular rooms. Our data shows that increasing the volume of the block increases the peak amplitude of the TR focus. The research of Ribay *et al.*[29] showed that as absorption of the room was decreased (volume constant), A_p and τ increased but they made a general statement that A_p is proportional to τ and did not explicitly show how A_p should change when room volume is changed. Denison and Anderson[31] showed that as the volume of the room increased (absorption constant), A_p followed the relationship $e^{-\tau}$. Because τ is proportional to room volume for sound in air, the work of Denison and Anderson[31] suggests that as volume is increased that the A_p should decrease. Here, also it was found that τ is proportional to block volume for elastic waves. It is possible that the discrepancy of our findings with that of Denison and Anderson[31] is because the experiments here were conducted with elastic waves, whereas the work of Ribay *et al.*[29] and Denison and Anderson[31] were done with sound in rooms (longitudinal waves only). We expected the results of this experiment to be similar to the Denison and Anderson[31] findings because the process of changing the volume and keeping everything else the same was similar in both studies. However, loss of wave energy for sound in rooms is mostly due to wall absorption and spherical spreading (i.e., propagation losses are not dominant), but loss of wave energy for elastic waves in solids is due to propagation losses in addition to boundary reflection losses and spherical spreading.

The findings for A_p with increasing volume of the other two blocks and with deconvolution TR suggest that there is no clear relationship between A_p and volume. It is important to recall the normalization scheme used in this study. The reversed impulse responses are normalized with respect to their peak value before these signals are sent to the amplifier (on their way to the transducer sources) in order to maximize the amplification capacity of the amplifier without distorting the input signal (i.e., the reversed impulse responses). An analysis of the normalized, reversed impulse responses reveals that the peak used for normalization is never the peak corresponding to the direct sound. Since the source transducers were nominally 9 cm away from the focal location, the direct sound should arrive approximately 31 μs after emission. However, the largest peak in the reversed impulse response was often several hundred microseconds after the direct sound. In Fig. 3(b) for example, the peak of the signal occurs at 300 μs, long after the expected arrival of the direct sound. The impulse responses used by Denison and Anderson[31] were also always normalized by the peak value in their reversed impulse responses, but this peak always corresponded to the direct sound. This information was not specified in their paper but was subsequently verified with the authors.

In an attempt to determine whether the peak normalization scheme employed here skews the relationship of A_p versus volume, a time reversal simulation scheme was developed. The TR process has been described as an autocorrelation process.[31,51] The focal signal is the autocorrelation of the impulse response between the source and the receiver (located at the focal location). With four sources in use, the four autocorrelation results performed with each of the four impulse responses between each source and the focal location may be summed to simulate the focal signal.

The unnormalized impulse responses (the raw result of the cross correlation of the chirp signal and the chirp response) between the i th transducer source and the focal location, IR_i, and the normalized versions (peak normalization) of these impulse responses, $\widehat{IR}_i$ (the hat symbol, $\widehat{\ }$, denotes peak normalization), will now be used to simulate focal signals. To simulate the focal signals, f, obtained in the current study for different volumes and cavity geometries, cross-correlations (nearly an autocorrelation) are used,

https://doi.org/10.1121/10.0005654

$$f = \sum_{\mathrm{i}} \frac{1}{T} \int_{-T/2}^{T/2} \widehat{IR_{\mathrm{i}}}(t) \cdot IR_{\mathrm{i}}(t+\tau)dt, \tag{4}$$

where $T = 32\,\mathrm{ms}$ is twice the length of either impulse response. The peak focal amplitude, A_p, of these TR focal signal simulations is then determined as a function of volume for each cavity geometry. Note that Eq. (4) utilizes a normalized impulse response and an unnormalized impulse response in the cross correlation operation since this study sent a normalized, reversed impulse response from each source that traveled through the system (hence the unnormalized impulse response). The summation $\sum_{\mathrm{i}}$ simulates the superposition of the TR focusing produced by each of the four sources.

In order to simulate the removal of the normalization based on the peak of the reversed impulse response, an autocorrelation of the unnormalized impulse responses is used,

$$f = \sum_{\mathrm{i}} \frac{1}{T} \int_{-T/2}^{T/2} IR_{\mathrm{i}}(t) \cdot IR_{\mathrm{i}}(t+\tau)dt. \tag{5}$$

The use of unnormalized impulse responses implies that an unnormalized impulse response is what is time reversed and broadcast by the sources. The direct sound arrivals from each source to the receiver location during the forward step are not easily distinguishable from other early reflection arrivals, though the amplitude of the direct sound arrival should remain the same for a given source to receiver combination irrespective of the block volume. In the previous section, we reported that the direct sound amplitudes are similar in amplitude from each source since the sources are each positioned at similar distances from the receiver location. Thus, Eq. (5) may not technically simulate a normalization based on the direct sound because the direct sound was not identified and used to normalize the RIRs. The effect of the peak normalization is removed though and Eq. (5) should yield results very similar to what would be expected if the normalization was based on the direct sound amplitudes. The peak focal amplitude, A_p, of these TR focal signal simulations is then determined as a function of volume for each cavity geometry.

Figure 5 also displays the results of using Eq. (5) to simulate the results that would be obtained for A_p versus volume if the peak normalization scheme was not used. Thus the "Peak Norm." data in Fig. 5 was obtained when using peak normalization and these results were discussed in Sec. III and the beginning of Sec. IV. The "No Norm." data comes from the results using Eq. (5). It should be noted that when Eq. (4) was used to extract A_p versus volume, that the results were essentially identical to those displayed in Fig. 5 (the black colored data points) when the set of results was linearly scaled down to appropriate values. For traditional TR without peak normalization, the correlation coefficients for the rectangular, cylindrical, and ergodic blocks are $R = -0.52$, $R = -0.75$, and $R = -0.94$, respectively. For deconvolution TR without peak normalization, the correlation coefficients for the rectangular, cylindrical, and ergodic blocks are $R = -0.94$, $R = -0.87$, and $R = -0.85$, respectively. These stronger, negative correlation coefficient results suggest a decreasing A_p as the volume increases. This is more in line with the findings of Denison and Anderson.[31] Thus, it appears that the normalization scheme employed makes a big difference as to whether one would expect a correlation between A_p and the volume of the cavity/block. It should be noted that a linear fit correlation was analyzed above rather than a fit to e^{-V}, where V is volume (recall that for rooms τ is proportional to V and it appears that this proportionality of τ and V holds for these blocks as well). There does appear to be a slight curvature that would correspond to an e^{-V} type slope for the ergodic cavity results. The e^{-V} (or $e^{-\tau}$ since τ is proportional to V) slope observed by Denison and Anderson locally appeared to be somewhat linear as it does here for the rectangular and cylindrical blocks. The variance in the data makes it difficult to confirm whether A_p decreases linearly with increasing volume or whether it falls off as e^{-V}. This variance is seen in both sets of data in Fig. 5 and either stems from imperfections in the experimental process as samples were cut down between measurement points, despite our careful efforts to maintain controls on the experimental conditions, or from changes to the modal response of the samples as one of the dimensions is changed (the modes may thus contribute differently to the focal amplitude). It must be remembered that Denison and Anderson explored a range of rooms with a volume change of 216 times from the smallest room to the largest one, whereas the blocks here were changed in volume by about a factor of 5. Hence a linear dependence might be expected for this relatively small overall change in volume.

Denison and Anderson[31] utilized a source and receiver that were placed towards the middle of every room and when the volume of the room was changed, the walls moved in all directions away from these transducers. Here, the sources and receiver were always at one end of the elastic cavity, while the opposite end of the cavity was moved closer and closer as the blocks were cut down. Denison was kind enough to rerun his simulations with the source and receiver always placed the same distance from one wall in his rooms, the room cross section remained the same, and he varied the volume only by moving the opposing wall further from the source and receiver. He found that this did not change the conclusions reported in Denison and Anderson—that A_p is proportional to $e^{-\tau}$. Thus, the position of the source and the receiver within the reverberant room does not appear to change the dependence of A_p on volume and we expect it not to change the dependence in elastic cavities either.

V. CONCLUSION

This study has found that the peak amplitude, A_p, of the TR focusing is consistently largest in the ergodic block, with the rectangular block yielding the lowest average A_p values. The temporal symmetry and full width at half maximum metrics were best in the cylindrical block and worst in the rectangular block (though the temporal symmetry values

for the cylindrical and ergodic blocks were very similar). The temporal quality, spatial clarity, and spatial quality of the TR focusing were highest in the ergodic block. In general, the ergodic block yielded the highest TR focusing amplitude and had the highest quality focusing performance. The spatial focusing generally improved with increasing volume of the blocks. Thus, the shape of the block used in a TR process does affect the TR focusing and so does the volume to a lesser extent. These conclusions were drawn from the traditional TR results and similar findings can be drawn from the deconvolution TR results. It does not appear that the reverberation time depends on the shape of the block. Additionally, the efficiency of the transducers used on each block were all fairly similar.

The TR focusing amplitude, A_p, as a function of the volume of the cavity depends on the normalization scheme employed prior to the broadcast of the reversed impulse response. When the impulse response is normalized with respect to its peak value, the dependence is often inconclusive among the various blocks and TR techniques used: sometimes A_p decreases with increasing volume, sometimes A_p increases with increasing volume, and sometimes it neither increases nor decreases with increasing volume. However, when the reversed impulse response is not normalized prior to broadcast, A_p consistently decreases with increasing volume, as Denison and Anderson[31] asserted when doing TR with audible sound in rooms of different sizes.

When designing a chaotic cavity for use in nondestructive evaluation of small parts or when transducers cannot be bonded onto the sample under test, the chaotic cavity should be made to have an ergodic shape and be fairly small in volume. For smaller volumes, the spatial focusing is slightly lower but A_p is larger. The ergodic cavity shape used here seems to be an ideal geometry since it affords flat surfaces that are ideal to bond transducers to, though machining this shape is not trivial.

ACKNOWLEDGMENTS

Funding provided by internal support from the BYU College of Physical and Mathematical Sciences is gratefully acknowledged. The authors also wish to thank Pierre-Yves Le Bas for his previous work in developing software that was used in this project, Michael Denison for running some additional simulations, Sarah Young for her assistance in getting started with this project, and Jeremy Peterson and his assistants for their work in machining the blocks and cutting them down.

[1]M. Fink, "Time reversed acoustics," Phys. Today **50**(3), 34–40 (1997).
[2]B. E. Anderson, M. Griffa, C. Larmat, T. J. Ulrich, and P. A. Johnson, "Time reversal," Acoust. Today **4**(1), 5–16 (2008).
[3]M. Scalerandi, A. S. Gliozzi, B. E. Anderson, M. Griffa, P. A. Johnson, and T. J. Ulrich, "Selective source reduction to identify masked sources using time reversal acoustics," J. Phys. D Appl. Phys. **41**, 155504 (2008).
[4]B. E. Anderson, T. J. Ulrich, M. Griffa, P.-Y. Le Bas, M. Scalerandi, A. S. Gliozzi, and P. A. Johnson, "Experimentally identifying masked sources applying time reversal with the selective source reduction method," J. Appl. Phys. **105**(8), 083506 (2009).
[5]C. S. Larmat, R. A. Guyer, and P. A. Johnson, "Time-reversal methods in geophysics," Phys. Today **63**(8), 31–35 (2010).
[6]B. E. Anderson, M. Griffa, T. J. Ulrich, and P. A. Johnson, "Time reversal reconstruction of finite sized sources in elastic media," J. Acoust. Soc. Am. **130**(4), EL219–EL225 (2011).
[7]B. E. Anderson, T. J. Ulrich, P.-Y. Le Bas, and J. A. Ten Cate, "Three-dimensional time reversal communications in elastic media," J. Acoust. Soc. Am. **139**(2), EL25–EL30 (2016).
[8]H. C. Song, "An overview of underwater time-reversal communication," IEEE J. Oceanic Eng. **41**(3), 644–655 (2016).
[9]L. P. Maia, A. Silva, and S. M. Jesus, "Environmental model-based time-reversal underwater communications," IEEE Access **6**, 10041–10051 (2018).
[10]P.-Y. L. Bas, T. J. Ulrich, B. E. Anderson, and J. J. Esplin, "A high amplitude, time reversal acoustic non-contact excitation (TRANCE)," J. Acoust. Soc. Am. **134**(1), EL52–EL56 (2013).
[11]B. E. Anderson, M. C. Remillieux, P.-Y. L. Bas, and, and T. J. Ulrich, "Time reversal techniques," in *Nonlinear Acoustic Techniques for Nondestructive Evaluation*, 1st ed., edited by T. Kundu (Springer and Acoustical Society of America, New York, 2018), Chap. 14, pp. 547–581.
[12]M. L. Willardson, B. E. Anderson, S. M. Young, M. H. Denison, and B. D. Patchett, "Time reversal focusing of high amplitude sound in a reverberation chamber," J. Acoust. Soc. Am. **143**(2), 696–705 (2018).
[13]A. Parvulescu and C. S. Clay, "Reproducibility of signal transmission in the ocean," Radio Elec. Eng. **29**, 223–228 (1965).
[14]C. S. Clay and B. E. Anderson, "Matched signals: The beginnings of time reversal," Proc. Mtg. Acoust. **12**, 055001 (2011).
[15]C. Draeger and M. Fink, "One-channel time-reversal in chaotic cavities: Theoretical limits," J. Acoust. Soc. Am. **105**(2), 611–617 (1999).
[16]C. Draeger, J.-C. Aime, and M. Fink, "One-channel time reversal in chaotic cavities: Experimental results," J. Acoust. Soc. Am. **105**(2), 618–625 (1999).
[17]A. M. Sutin, J. A. TenCate, and P. A. Johnson, "Single-channel time reversal in elastic solids," J. Acoust. Soc. Am. **116**(5), 2779–2784 (2004).
[18]T. J. Ulrich, P. A. Johnson, and A. Sutin, "Imaging nonlinear scatterers applying the time reversal mirror," J. Acoust. Soc. Am. **119**, 1514–1518 (2006).
[19]T. J. Ulrich, P. A. Johnson, and R. A. Guyer, "Interaction dynamics of elastic waves with a complex nonlinear scatterer through the use of a time reversal mirror," Phys. Rev. Lett. **98**, 104301 (2007).
[20]T. J. Ulrich, A. M. Sutin, T. Claytor, P. Papin, P.-Y. L. Bas, and J. A. Ten Cate, "The time reversed elastic nonlinearity diagnostic applied to evaluation of diffusion bonds," Appl. Phys. Lett. **93**, 151914 (2008).
[21]B. E. Anderson, M. Griffa, T. J. Ulrich, P.-Y. L. Bas, R. A. Guyer, and P. A. Johnson, "Crack localization and characterization in solid media using time reversal techniques," in *Proceedings of the 44th U.S. Rock Mechanics Symposium*, Salt Lake City, UT (June 27–30, 2010), Paper No. 10–154.
[22]B. E. Anderson, M. Griffa, P.-Y. L. Bas, T. J. Ulrich, and P. A. Johnson, "Experimental implementation of reverse time migration for nondestructive evaluation applications," J. Acoust. Soc. Am. **129**(1), EL8–EL14 (2011).
[23]S. M. Young, B. E. Anderson, M. L. Willardson, P. E. Simpson, and P.-Y. L. Bas, "A comparison of impulse response modification techniques for time reversal with application to crack detection," J. Acoust. Soc. Am. **145**(5), 3195–3207 (2019).
[24]S. M. Young, B. E. Anderson, S. M. Hogg, P.-Y. L. Bas, and M. C. Remillieux, "Nonlinearity from stress corrosion cracking as a function of chloride exposure time using the time reversed elastic nonlinearity diagnostic," J. Acoust. Soc. Am. **145**(1), 382–391 (2019).
[25]C. Larmat, J.-P. Montagner, M. Fink, Y. Capdeville, A. Tourin, and E. Clévédé, "Time-reversal imaging of seismic sources and applications to the great Sumatra earthquake," Geophys. Res. Lett. **33**, L19312, https://doi.org/10.1029/2006GL026336 (2006).
[26]C. Larmat, J. Tromp, Q. Liu, and J.-P. Montagner, "Time-reversal location of glacial earthquakes," J. Geophys. Res. **113**, B09314, https://doi.org/10.1029/2008JB005607 (2008).
[27]R. K. Ing and N. Quieffin, "In solid localization of finger impacts using acoustic time-reversal process," Appl. Phys. Lett. **87**(20), 204104 (2005).
[28]D. Vigoureux and J.-L. Guyader, "A simplified time reversal method used to localize vibrations sources in a complex structure," Appl. Acoust. **73**(5), 491–496 (2012).
[29]G. Ribay, J. de Rosny, and M. Fink, "Time reversal of noise sources in a reverberation room," J. Acoust. Soc. Am. **117**(5), 2866–28720 (2005).

[30]M. H. Denison and B. E. Anderson, "The effects of source placement on time reversal focusing in rooms," Appl. Acoust. **156**, 279–288 (2019).
[31]M. H. Denison and B. E. Anderson, "Time reversal acoustics applied to rooms of various reverberation times," J. Acoust. Soc. Am. **144**(6), 3055–3066 (2018).
[32]B. E. Anderson, M. Clemens, and M. L. Willardson, "The effect of transducer directionality on time reversal focusing," J. Acoust. Soc. Am. **142**(1), EL95– EL101 (2017).
[33]T. S. Furlong, B. E. Anderson, B. D. Patchett, and S. D. Sommerfeldt, "Active noise control using remotely placed sources: Application to magnetic resonance imaging noise and equivalence to the time reversal inverse filter," Appl. Acoust. **176**, 107902 (2021).
[34]J.-L. Thomas, F. Wu, and M. Fink, "Time reversal mirror applied to lithotripsy," Ultrason. Imag. **18**, 106–121 (1996).
[35]J.-L. Thomas and M. Fink, "Ultrasonic beam focusing through tissue inhomogeneities with a time reversal mirror: Application to transskull therapy," IEEE Trans. Ultrason. Ferroelect. Freq. Control **43**(6), 1122–1129 (1996).
[36]M. Tanter, J.-L. Thomas, and M. Fink, "Focusing and steering through absorbing and aberating layers: Application to ultrasonic propagation through the skull," J. Acoust. Soc. Am. **103**(5), 2403–2410 (1998).
[37]S. Dos Santos and Z. Prevorovsky, "Imaging of human tooth using ultrasound based chirp-coded nonlinear time reversal acoustics," Ultrasonics **51**(6), 667–674 (2011).
[38]T. Shimura, Y. Watanabe, H. Ochi, and H. C. Song, "Long-range time reversal communication in deep water: Experimental results," J. Acoust. Soc. Am. **132**(1), EL49–EL53 (2012).
[39]G. Montaldo, D. Palacio, M. Tanter, and M. Fink, "Time reversal kaleidoscope: A smart transducer for three-dimensional ultrasonic imaging," Appl. Phys. Lett. **84**(19), 3879–3881 (2004).
[40]N. Quieffin, S. Catheline, R. K. Ing, and M. Fink, "2D pseudo-array using an ultrasonic one channel time-reversal mirror," in *Proceedings of the IEEE Ultrasonics Symposium*, Montreal, Canada (August 24–27, 2004), pp. 801–804.
[41]O. Bou Matar, Y. Li, S. Delrue, and K. Van Den Abeele, "Optimization of chaotic cavity transducers to nonlinear elastic imaging," in *Proceedings of the 10th French Congress on Acoustics*, Lyon, France (April 12–16, 2010).
[42]B. Van Damme, K. Van Den Abeele, Y. Li, and O. Bou Matar, "Time reversed acoustics techniques for elastic imaging in reverberant and non-reverberant media: An experimental study of the chaotic cavity transducer concept," J. Appl. Phys. **109**, 104910 (2011).
[43]P.-Y. Le Bas, T. J. Ulrich, B. E. Anderson, and J. Esplin, "Toward a high power non-contact acoustic source using time reversal," Acoust. Soc. Am. ECHOES Newslett. **22**(3), 7–8 (2012).
[44]S. Delrue, P.-Y. Le Bas, T. J. Ulrich, B. Anderson, and K. Van Den Abeele, "First simulations of the candy can concept for high amplitude non-contact excitation," Proc. Mtg. Acoust. **16**, 045019 (2012).
[45]B. E. Anderson, T. J. Ulrich, and P.-Y. Le Bas, "Improving the focal quality of the time reversal acoustic noncontact source using a deconvolution operation," Proc. Mtg. Acoust. **19**, 065069 (2013).
[46]S. Delrue, K. Van Den Abeele, P.-Y. Le Bas, T. J. Ulrich, and B. E. Anderson, "Simulations of a high amplitude air coupled source based on time reversal," in *Proceedings of the International Congress on Ultrasonics*, Singapore (May 2–5, 2013), pp. 591–596.
[47]P.-Y. Le Bas, M. C. Remillieux, L. Pieczonka, J. A. Ten Cate, B. E. Anderson, and T. J. Ulrich, "Damage imaging in a laminated composite plate using an air-coupled time reversal mirror," Appl. Phys. Lett. **107**, 184102 (2015).
[48]O. I. Lobkis and R. L. Weaver, "Coda-wave interferometry in finite solids: Recovery of P-to-S conversion rates in an elastodynamic billiard," Phys. Rev. Lett. **90**(25), 254302 (2003).
[49]N. Quieffin, "Etude du rayonnement acoustique de structures solides: Vers un système d'imagerie haute resolution" ("Study of the acoustic radiation of solid structures: Towards a high resolution imaging system"), Ph.D. thesis, Universite Pierre et Marie Curie, Paris, France, 2004.
[50]M. C. Remillieux, B. E. Anderson, T. J. Ulrich, P.-Y. Le Bas, and C. Payan, "Depth profile of a time-reversal focus in an elastic solid," Ultrasonics **58**, 60–66 (2015).
[51]M. Tanter, J.-L. Thomas, and M. Fink, "Time reversal and the inverse filter," J. Acoust. Soc. Am. **108**, 223–234 (2000).
[52]T. Gallot, S. Catheline, P. Roux, and M. Campillo, "A passive inverse filter for Green's function retrieval," J. Acoust. Soc. Am. **131**, EL21–EL27 (2012).
[53]B. E. Anderson, J. Douma, T. J. Ulrich, and R. Snieder, "Improving spatio-temporal focusing and source reconstruction through deconvolution," Wave Motion **52**, 151–159 (2015).
[54]G. Montaldo, P. Roux, A. Derode, C. Negreira, and M. Fink, "Ultrasound shock wave generator with one-bit time reversal in a dispersive medium, application to lithotripsy," Appl. Phys. Lett. **80**(5), 897–899 (2002).
[55]C. Heaton, B. E. Anderson, and S. M. Young, "Time reversal focusing of elastic waves in plates for educational demonstration purposes," J. Acoust. Soc. Am. **141**(2), 1084–1092 (2017).
[56]A. S. Gliozzi, M. Scalerandi, and P. Antonaci, "One-channel time-reversal acoustics in highly attenuating media," J. Phys. D: Appl. Phys. **46**, 135502 (2013).
[57]T. J. Ulrich, M. Griffa, and B. E. Anderson, "Symmetry-based imaging condition in time reversed acoustics," J. Appl. Phys. **104**(6), 064912 (2008).
[58]R. Weaver, "The unreasonable effectiveness of random matrix theory for the vibrations and acoustics of complex structures," in *New Directions in Linear Acoustics and Vibration*, edited by M. Wright and R. Weaver (Cambridge University Press, Cambridge, UK, 2010), Chap. 3, pp. 42–58; 74–75.
[59]R. Weaver, "Wave chaos in elastodynamics," in *Waves and Imaging Through Complex Media*, edited by P. Sebbah (Springer Science & Business Media, New York, 2001), Chap. 3, pp. 141–186.
[60]R. Weaver, "Spectral statistics in elastodynamics," J. Acoust. Soc. Am. **85**(3), 1005–1013 (1989).